CRYSTAL GROWTH & DESIGN

Article

pubs.acs.org/crystal

Influence of Solubilizing Group Removal Rate on the Morphology and Crystallinity of a Diketopyrrolopyrrole-Based Compound

Shabi Thankaraj Salammal,*[,†] Jean-Yves Balandier,[†] Saroj Kumar,[‡] Erik Goormaghtigh,[‡] and Yves Henri Geerts[†]

[†]Laboratory of Polymer Chemistry and [‡]Laboratory for Structure and Function of Biological Membrane, Faculté des Sciences, Université Libre de Bruxelles (ULB), Boulevard du Triomphe, 1050 Brussels, Belgium

Supporting Information

ABSTRACT: Thermally cleavable solubilizing groups have been introduced on a π-conjugated core, which can be cleaved and volatilized via heat treatment directly after the thin film fabrication. The X-ray and atomic force microscopic investigations of "3,6-di(2,2′-bithiophen-5-yl)pyrrolo[3,4-*c*]pyrrole-1,4-(2*H*,5*H*)-dione" (DPP-4T) synthesized from its precursor (di-*tert*-butyl-3,6-di(2,2′-bithiophen-5-yl)-1,4-dioxo-pyrrolo[3,4-*c*]pyrrole-2,5-(1*H*,4*H*)-dicarboxylate) through thermal conversion reveals that the solubilizing group removal rate plays a crucial role on the ultimate grain size and crystallinity of the final compound (DPP-4T). This means that, when the heating rate is decreased from 50 to 0.1 °C/min, the crystallinity of DPP-4T powder decreases from 49% to 34%, and the grain size of DPP-4T film reduces from 976 to 344 nm. The crystallite size of the films can be further reduced to 185 nm by decarboxylating the films isothermally at 120 °C. The Fourier transform infrared spectra reveals that the reduction of crystallinity with the heating rate could be attributed to the trapping of gaseous byproducts inside the lattice, during the decarboxylation of the solubilizing group. The increment in intermolecular N−H···O═C hydrogen bond length together with the trapped gaseous byproducts results in a blue shift in the UV−vis absorption spectra while decreasing the heating rate as well as the isothermal decarboxylation temperature.

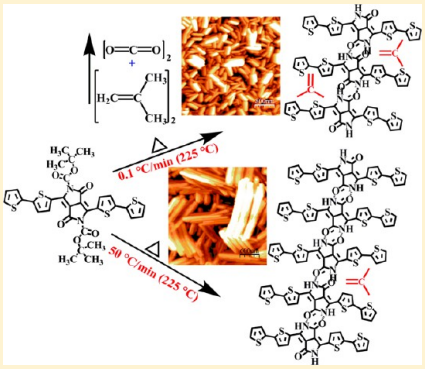

INTRODUCTION

The excellent electrical and optical properties of dioxo-3,6-diarylpyrrolo[3,4-*c*]pyrroles, commonly abbreviated as DPP, along with their environmentally benign features have found their profound application in optoelectronic sectors.[1−3] The DPP-based polymers and small molecules have been generally used to fabricate organic solar cells[1,2,4] due to their ease at tuning the band gap by flanking the electron-deficient pyrrolopyrrole with the electron-rich aromatic moieties, such as thiophene or thienothiophene, phenyl, etc.[5,6] Such DPP-based compounds are not soluble in common organic solvents because of strong intermolecular N−H···O═C hydrogen bonds and $\pi-\pi$ interactions, which complicate the fabrication of organic electronic devices further.[1,7,8] In most cases, the solubility of such conjugated molecules is obtained through grafting the flexible side chains. Though the significance of alkyl side chains enables us to engineer the crystal structure and resulting thin film morphology, their insulating properties tend to hamper the realization of efficient electronic devices.[9−11] Moreover, these solubilizing groups also promote the soft characteristics of functional organic materials, inducing conformational defects and polymorphism.[10] Therefore, the devices are in need of different morphologies to meet their respective applications. For example, edge- and face-on oriented crystallites are mandatory for the fabrication of efficient organic field effect transistors (OFETs) and solar cells, respectively.[9,12] It has been documented that the aforementioned problems can be solved by grafting the solubilizing groups such as *t*-butoxycarbonyl (*t*-BOC) and ester or tetrahydropyran, which can be cleaved and volatilized via thermal or acid treatment directly after the film preparation.[7,13−17] Moreover, the insolubility of thermally or acid-treated films assists to fabricate heterostructures without dissolving the prepatterned layers through solution processing techniques.[15,18]

Various solubilizing group free organic small molecules and polymers, such as dioxo-3,6-diphenylpyrrolo[3,4-*c*]pyrrole (DPP-phenyl), dinaphtho[2,3-*b*:2′,3′-*f*]thieno[3,2-*b*]thiophene (DNTT), polythiophenes, poly(*p*-phenylene vinylene), pentacene, hexane, and tetrabenzoporphyrin (BP), have been synthesized from their precursors via heat treatment.[7,13,14,19−21] For example, insoluble pentacene could be synthesized from its precursor (13,6-*N*-sulfinylacetamidopentacene) through a thermochemical process, which releases *N*-sulfinylamide during the decomposition of its solubilizing group.[22] Similarly, Soeda et al. have successfully grown single crystalline pentacene and DNTT platelets during the removal of the solubilizing group from their precursor solution via heat treatment.[13] On the

Received: October 30, 2013
Revised: November 25, 2013
Published: December 2, 2013

dx.doi.org/10.1021/cg401625p | *Cryst. Growth Des.* 2014, 14, 339−349

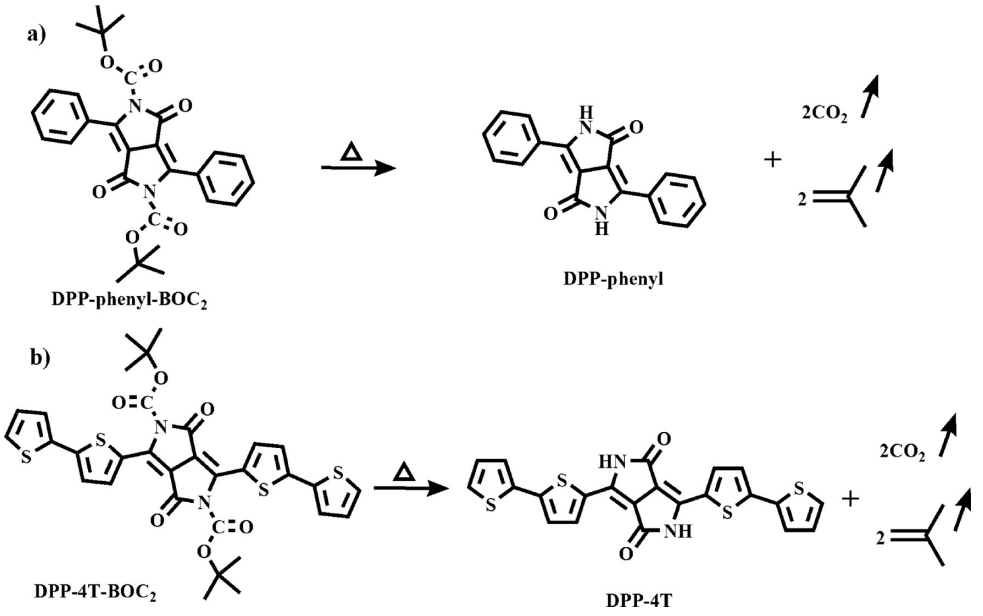

Figure 1. Chemical structure of (a) DPP-phenyl and (b) DPP-4T obtained upon the thermal conversion of their precursors DPP-phenyl-BOC_2 and DPP-4T-BOC_2, respectively.

contrary, the same pentacene films obtained from its precursor films through the thermochemical process results in smaller crystallites.[23] However, there seems to be a lack of knowledge on how the precursors get converted, and the interplay between the removal rate of the solubilizing group and the morphology and crystallinity of the films produced. Generally, the precursor tends to produce amorphous or crystalline films, whereas the thermally converted molecules tend to crystallize. So, how do nucleation and growth take place? How do films accommodate the density difference? How do the volatilized molecules escape from the lattice and how do they facilitate crystal growth? Though such factors could be believed as fundamental issues, their understanding and address has to be emphasized strongly to visualize highly efficient devices. Until now, most of such studies were often conducted with the aim to fabricate efficient devices rather than to address these fundamental issues.[3,14,19,22] For example, Søndergaard et al. have reported that the fast and slow removal rate of the solubilizing group reduces the solar cell efficiency.[14]

Since the performances of organic electronic devices, such as OFETs,[24] solar cells,[2,4,25] etc., are depending on the morphology and crystallinity of the functional materials, it seems opportune to conduct morphological and structural studies on a model system that was obtained from its precursor through the thermochemical process. To that end, the di-*tert*-butyl-3,6-di(2,2′-bithiophen-5-yl)-1,4-dioxopyrrolo[3,4-*c*]-pyrrole-2,5-(1*H*,4*H*)-dicarboxylate (DPP-4T-BOC_2) precursor has been selected from the structural family of DPP. These DPP derivatives are readily synthesized and are well-known for their thermal stability, allowing to set aside the problems of decomposition upon thermal conversion.[3,7] The best known member of the DPP family is DPP-phenyl that can be obtained from its precursor (di-*tert*-butyl-1,4-dioxo-3,6-diphenylpyrrolo-[3,4-*c*]pyrrole-2,5-(1*H*,4*H*)-dicarboxylate (DPP-phenyl-BOC_2)) by thermal conversion, as illustrated in Figure 1a. Nevertheless, DPP-phenyl has not been chosen for our study because the twist conformation of phenyl reduces the effective conjugation and results in a blue shift as compared to the DPP-substituted with thiophene moieties.[1,26,27] Hence, DPP grafted with thiophene moieties is widely used to fabricate various organic electronic devices;[1,2] so DPP-4T-BOC_2 has been chosen as a precursor for this piece of work. The thermal conversion of DPP-4T-BOC_2 into 3,6-di(2,2′-bithiophen-5-yl)pyrrolo[3,4-*c*]pyrrole-1,4-(2*H*,5*H*)-dione (DPP-4T) is schematically illustrated in Figure 1b. The *t*-BOC (solubilizing group) decomposes into isobutylene and CO_2 around 180 °C (Figure 1).[7] Here, we have investigated the effect of decarboxylation rate on the morphology and crystallinity of DPP-4T films by employing atomic force microscopic (AFM) and X-ray diffraction analyses, respectively. The decarboxylation rate of the solubilizing group was controlled by two ways: (i) heating the precursor up to 225 °C with various heating rates (0.1−50 °C/min) and (ii) isothermally decarboxylating the precursor at various temperatures. The results have been additionally confirmed by optical (Fourier transform infrared spectroscopy (FTIR) and UV−vis absorption) and nuclear magnetic resonance (NMR) spectroscopic analyses.

EXPERIMENTAL DETAILS

Thin Film Preparation. The synthesis of high-purity DPP-4T-BOC_2 and the crystal structure of its polymorphic phases can be found elsewhere.[27] Highly uniform precursor films (DPP-4T-BOC_2) were spin-coated with various thicknesses on the cleaned glass substrates (2 × 2 cm^2). The substrates were cleaned sequentially with dilute liquid detergent (RBS T 105), isopropanol, and acetone for 15 min in each, using an ultrasonic bath. The substrates were further cleaned with UV−ozone cleaner in order to remove the organic impurities left over the substrate surface. The precursor solutions with various concentrations were prepared by dissolving 10 mg of DPP-4T-BOC_2 in 1, 2, 3, and 4 mL of $CHCl_3$. The solution was stirred continuously at 50 °C for 3 h using a hot plate. The concentration of the solution was varied in order to prepare mostly amorphous thick films with good surface uniformity. Prior to the film preparation, the solution was cooled down to room temperature (RT). The solution was filtered using a syringe filter that contains a 0.2 μm pore size. Except for the concentration of the solution, spinning speed (1000 rpm), duration (60 s), and amount of dropped solutions (170 μL) were kept constant during the spin-coating process.

dx.doi.org/10.1021/cg401625p | *Cryst. Growth Des.* 2014, 14, 339−349

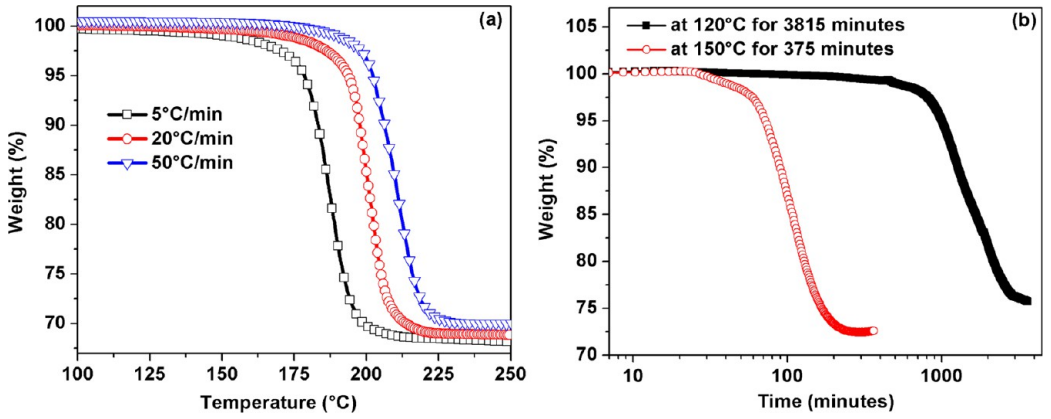

Figure 2. TGA curves of DPP-4T-BOC_2 collected with (a) various heating rates and (b) isothermally decarboxylated at 120 and 150 °C.

Solvent Vapor Annealing (SVA). SVA was employed to increase the crystallinity of DPP-4T-BOC_2 films, as reported by us earlier.[27] The films were exposed to the $CHCl_3$ vapor for a day.

Decarboxylation of the Films and Powders of DPP-4T-BOC_2. The as-spin-coated films were decarboxylated using a muffle furnace with various heating rates (from 0.1 to 50 °C/min). It was difficult to control the temperature overshoot while increasing the heating rate. The furnace was overheated to a maximum of up to 20 °C from the set point, while the heating rate was employed around 50 °C/min. The films were heated up to 225 °C and then waited for 30 min to complete the decarboxylation reaction. A set of films were decarboxylated isothermally at 120 and 150 °C for 48 and 15 h, respectively. A film was also decarboxylated by suddenly exposing at 225 °C for 30 min in order to avoid the crystallization of DPP-4T-BOC_2 during heating. In addition, 25 mg of DPP-4T-BOC_2 powders was decarboxylated under the same condition as used for the films in order to calculate the percentage of crystallinity through the X-ray diffraction technique.

Thermogravimetric Analysis (TGA). Prior to the decarboxylation, TGA analysis was carried out using a PYRIS 6 TGA (PerkinElmer) to investigate the decarboxylation temperature and the rate of the solubilizing group under a N_2 atmosphere.

X-ray Analysis of Powders and Films. The grazing incidence in-plane X-ray diffraction (GID) analyses were carried out using a Rigaku machine (UltimaIV). The incidence angle of the X-ray beam was fixed at 0.22° in order to increase the scattering signal of the films. In addition, the in situ out-of-plane X-ray diffraction (specular) analysis was carried out using a D8 Advance machine (Bruker AXS) for the better understanding of the temperature-dependent decarboxylation of *t*-BOC. Noteworthy, it was not possible to in situ monitor the evolution of the DPP-4T phase upon the thermal conversion of DPP-4T-BOC_2, due to their weak scattering. Therefore, the weakening of a Bragg peak of the DPP-4T-BOC_2 film was monitored upon heating. The powder pattern of DPP-4T was also recorded using the same machine under specular condition. The X-ray reflectivity (XRR) profiles of the films were also recorded using the D8 machine under specular condition. In both the cases, we have used the laboratory sources (Cu tube). Independent from the machines, the step size was kept constant at 0.02° throughout the diffraction analyses, and it was further reduced to 0.006° for the XRR analysis.

Crystallinity Calculation. The percentage of crystallinities of DPP-4T powders was extracted from the corresponding diffractograms using a simple relation given in the Supporting Information (SE1).[28] However, the true value of crystallinity could not be extracted by avoiding incoherent scatterings, such as Compton scattering, Debye–Waller factor, and air scattering, due to the lack of monochromator to filter the copper $K\beta$ as well as the absence of Bragg reflections at higher angles.[28,29] Moreover, it was not possible to collect the diffractogram above 60° because of the geometrical restriction of the goniometer. More details about the percentage of crystallinity calculation can be found in the Supporting Information.

Electron Density Calculation. The electron densities of the films were calculated using the equation given in the Supporting Information (SE2) by extrapolating the critical angle of the films (α_{fi}) from the corresponding XRR curves.[30]

Infrared Spectroscopic Analysis. The FTIR spectra of the films were recorded by placing them on a diamond attenuated total reflectance (ATR) element. The spectra were recorded at 4 cm^{-1} resolution using a Bruker Equinox 55 FTIR spectrometer equipped with a HgCdTe detector. The experiments were performed at RT using the spectrometer software OPUS. For each spectrum, 256 scans were collected, and the background spectrum was also recorded before performing each measurement. All the experiments were repeated at least three times. We have continuously purged the sample compartment and the instrument with dry air.

Nuclear Magnetic Resonance Analysis. ^1H NMR (300 MHz) and ^{13}C NMR (75 MHz) were recorded using a Bruker Advance 300 spectrometer. Chemical shifts are given in ppm and coupling constants *J* in hertz. The residual signal of the solvent was taken as an internal reference.

Atomic Force Microscopic Analysis. The surface morphologies of the films were analyzed using a Nanoscope III Scanning Probe Microscope, under tapping mode.

Thermal Gradient. Decarboxylation of DPP-4T-BOC_2 single crystals were in situ monitored upon heating using a polarized optical microscope (POM), Nikon Eclipse 80i (without crossed polarizers). For this purpose, a Linkam GS350 temperature gradient system integrated with the POM microscope was used. The heating stage was made up of two independent heaters separated by a distance of 2.5 mm.[31] The single crystals of DPP-4T-BOC_2 were decarboxylated under a thermal gradient by keeping one heater at below the decarboxylation temperature (90 °C) and the second one at 170 °C. The crystals were dragged from the cold zone to the hot zone with various pulling rates.

UV–vis Absorption Spectroscopic Analysis. UV–vis absorption spectra of the films were recorded over a range of 200–900 nm under ambient conditions using an Agilent 8453 spectrometer.

RESULTS AND DISCUSSION

TGA Analysis of DPP-4T-BOC_2 Powder. First of all, TGA analysis of the precursor (DPP-4T-BOC_2) powder was carried out to investigate the thermochemical properties, such as decarboxylation temperature (decomposition of *t*-BOC), decarboxylation rate, and the decomposition temperature of DPP-4T. The DPP-4T-BOC_2 powders were decarboxylated with various heating rates (5, 20, and 50 °C/min). Because of the limitation of the equipment, we had difficulty in controlling the heating rate beyond 50 °C/min and below 5 °C/min. Figure 2a clearly depicts that the decarboxylation temperature and the rate are depending on the heating rate applied. The decarboxylation temperature increases from 178.2 to 200.8 °C

dx.doi.org/10.1021/cg401625p | *Cryst. Growth Des.* 2014, 14, 339–349

while increasing the heating rate from 5 to 50 °C/min (Table 1). Moreover, the decarboxylation rate was found to increase as a function of heating rate. To be more precise, ~7.1 mg of DPP-4T-BOC_2 was found to consume 159 and 22 s to complete their decarboxylation reactions, while the applied heating rate was held at 5 and 50 °C/min, respectively (Table 1). The duration of decarboxylation (rate) was then calculated by extrapolating the starting and end point of the decarboxylation reaction from the TGA curve (as the heating rates are known). Moreover, the percentage of weight loss during the decarboxylation process (Table 1; average weight loss = 30.6%) was found to be well in agreement with the calculated value (calculated weight loss = 30.1%), which is equivalent to the loss of two molecules of carbon dioxide and two molecules of isobutylene (Figure 1).[7] Therefore, this ensures the reaction to be successful and complete. Also, DPP-4T was found to be thermally stable for a wide range of temperatures and decomposes around ~460 °C, which can be confirmed through the presence of solid byproducts in the TGA pan after heating to 600 °C (Supporting Information, Figure S1).

Table 1. Influence of Heating Rate on the Decarboxylation Temperature, Percentage of Weight Loss, and Time Taken to Finish the Decarboxylation Reaction As Observed from TGA

heating rate (°C)	decarboxylation temperature (±0.5 °C)	duration of decarboxylation reaction (±2 s)	% of weight loss during decarboxylation (±0.5)
5	178.2	159	30.5
20	192.9	43	30.9
30	194.1	24	30.0
50	200.8	22	30.3

In addition, ≈ 6 mg of precursor powders was isothermally decarboxylated at 120 and 150 °C in order to understand the influence of temperature on the decomposition rate of *t*-BOC (Figure 2b). Here, the rate of the decarboxylation reaction was found to decrease as a function of temperature. For instance, while decarboxylating ≈6 mg of precursor powders isothermally at 120 and 150 °C, the decarboxylation reaction persisted for 2357 and 158 min, respectively. Interestingly, the percentage of weight loss was noted to decrease with the decarboxylation temperature; i.e., it decreases from 27.7% to 24.2% while decreasing the isothermal decarboxylation temperature from 150 to 120 °C, which is far less than the expected weight loss of 30.1%. The NMR spectra collected for the DPP-4T-BOC_2 powder decarboxylated isothermally at 120 °C for various time scales confirm the completion of decarboxylation reaction after 2880 min (2 days) of annealing (see later the NMR analysis). Therefore, the decrease of weight loss together with the decarboxylation temperature is not associated with the incompletion of the decarboxylation reaction, but it could be due to the trapping of gaseous byproducts inside the DPP-4T crystallites during the decarboxylation of the solubilizing groups (as observed from the FTIR spectra (see Figure 6)).[19]

X-ray Analysis of DPP-4T-BOC_2 (Precursor) Films. The main aim of this article is to understand the role of *t*-BOC removal rate from the precursor film on the crystallinity and morphology of DPP-4T films. Therefore, DPP-4T-BOC_2 films with various thicknesses were first spin-coated on the cleaned substrates of SiO_2. Especially, the concentration of the solution was increased to attain mostly amorphous thick films with good surface homogeneity. The XRR technique was employed to measure the thicknesses of the films. The thicknesses of the films were calculated from the obtained Kiessig fringes, and the average values are given in Figure 3a.[30] Here, the thicknesses of the films were found to increase with the concentration of the solution. Moreover, the decrease in the (002) reflection of DPP-4T-BOC_2 with increasing the concentration of the solution depicts the decrease in crystallinity of the films (Figure 3b). The whole diffractogram of the as-spin-coated DPP-4T-BOC_2 films from the range of Q_z = 0.4–2.3 $Å^{-1}$ is shown in the Supporting Information (Figure S2). The absence of any other Bragg reflections rather than the (002) and an amorphous halo confirms the decrease in crystallinity of the films while increasing the concentration of the solution. Such a sort of decrease in crystalline quality of DPP-4T-BOC_2 films could be attributed to the higher viscosity in the concentrated solution. The film spin-coated using the concentration 10 mg/mL has been used for further investigations because of its thickness (59 nm) and mostly amorphous nature.

X-ray Analysis of DPP-4T Films Obtained Through the Thermal Conversion of Their Precursor. Prior to decarboxylating the DPP-4T-BOC_2 films, the initiation of decarboxylation temperature and durations were investigated through in situ X-ray diffraction analysis. To that end, mostly amorphous (as-spin-coated) and highly crystalline films were used to investigate the initial physical state of the precursor

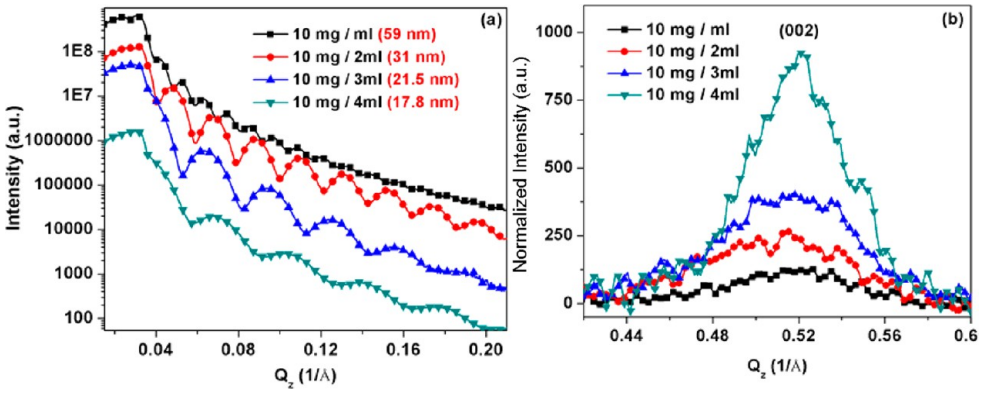

Figure 3. (a) XRR (shifted along the ordinate axis by adding certain values for clearer presentation) and (b) X-ray specular diffraction (normalized to the thickness) profiles of DPP-4T-BOC_2 as-spin-coated films using various concentrations.

dx.doi.org/10.1021/cg401625p | *Cryst. Growth Des.* 2014, 14, 339–349

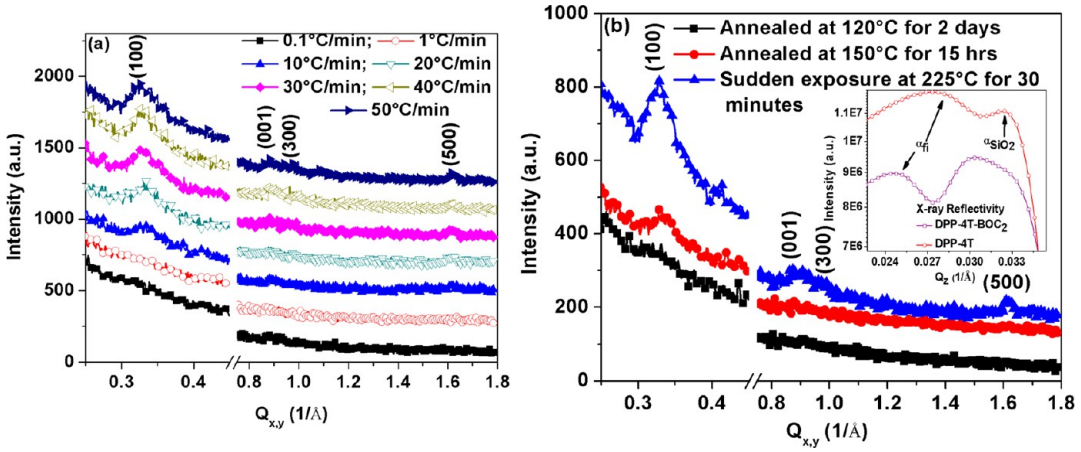

Figure 4. In-plane scattering patterns of DPP-4T films obtained from their precursor films through thermal conversion: (a) with different heating rates (heated up to 225 °C) and (b) the films decarboxylated isothermally at various temperatures. Inset of (b) shows the XRR curves of DPP-4T-BOC_2 and DPP-4T films.

films, when subjected to the decarboxylation reaction. Therefore, the mostly amorphous DPP-4T-BOC_2 film was easily converted to crystalline film, through SVA treatment (Figure S3, Supporting Information).[27] The appearance of much brighter crystallites in the SVA-treated DPP-4T-BOC_2 film as compared to the as-spin-coated one under crossed polarizers confirms the augmentation in crystalline perfection of SVA-treated film. The decay of the (002) reflection in the as-spin-coated films (monoclinic phase) and that of the (100) reflection of the SVA-films (triclinic phase) of DPP-4T-BOC_2 were monitored while isothermally annealing at various temperatures. The decrease in scattering intensity of the DPP-4T-BOC_2 phase upon heating as well as during the isothermal process confirms the conversion of DPP-4T-BOC_2 into DPP-4T. It clearly indicates that *t*-BOC starts to cleave around 90 °C from the as-spin-coated films and it further increased to 115 °C in the case of SVA-films (Figure S4, Supporting Information). The rise in decarboxylation temperature of the SVA-film might be due to the increased lattice energy, resulting from the formation of crystallites after the SVA treatment (Figure S3, Supporting Information).[27] The SVA-film took ≈2 days to complete the decarboxylation reaction while annealing isothermally at 115 °C. Henceforth, 120 °C was chosen as a minimum temperature to decarboxylate the films completely. For further investigations, the ≈59 nm thick mostly amorphous as-spin-coated DPP-4T-BOC_2 films have been used.

The 59 nm thick DPP-4T-BOC_2 film was observed to get reduced to 36 nm after the decarboxylation process, which was independent from the heating rates employed. The thickness of the DPP-4T film was much less than the expected value of 41.2 nm, which is equivalent to the loss of two molecules of carbon dioxide and two molecules of isobutylene from the DPP-4T-BOC_2 upon heating (totally 30.1%). It could be assigned to the close-packing of DPP-4T while compared with the DPP-4T-BOC_2 (as evident from the increased electron density values of DPP-4T on par with the DPP-4T-BOC_2).[32] Generally, the critical angle that is directly related to the electron density of the film was observed to shift toward higher Q_z after the decarboxylation process (inset of Figure 4b). The electron densities of the films were calculated by extrapolating the α_{fi} from the XRR curves.[30] It was noted to increase from 0.43 $Å^{-3}$ (DPP-4T-BOC_2 film) to 0.49 $Å^{-3}$ (DPP-4T) after the removal of the solubilizing group.

The specular diffraction patterns of DPP-4T films obtained through the thermal conversion of their precursor with various heating rates are shown in Figure S5 (Supporting Information); however, it did not provide any Bragg reflections. Therefore, the GID patterns of the films were collected and are shown in Figure 4. The Bragg reflections were found to be absent in the films decarboxylated with the heating rates of 0.1 and 1 °C/min. The Bragg reflections started to evolve on increasing the heating rate further (Figure 4a). The scattering intensity of all the reflections was noted to increase with the heating rate. Moreover, a similar tendency was also observed in the precursor films decarboxylated isothermally at various temperatures. For example, GID patterns of the films decarboxylated at 120, 150, and 225 °C are shown in Figure 4b. It clearly envisages the increase in crystallinity of DPP-4T films together with the heating rate as well as the isothermal decarboxylation temperature. It was not possible to extract the percentage of crystallinity from the obtained scattering patterns because of weak scattering. Therefore, ≈25 mg of DPP-4T-BOC_2 powders was decarboxylated under the same conditions in order to calculate the percentage of crystallinity from the corresponding X-ray diffractograms.

X-ray Analysis of DPP-4T Powder. The diffraction patterns of DPP-4T powders obtained through the thermal conversion of their precursor with various heating rates (heated up to 225 °C) and at various isothermal temperatures were collected to understand the role of *t*-BOC removal rate on the crystallinity of DPP-4T. The powder patterns of DPP-4T obtained through the thermal conversion of DPP-4T-BOC_2 isothermally at various temperatures (120, 150, and 225 °C) are shown in Figure 5. The scattering pattern of thermally synthesized DPP-4T from its precursor matches well with the scattering pattern of DPP-4T recrystallized using the solvent dimethyl sulfoxide (DMSO) (Figure S6c, Supporting Information). However, the absence of any Bragg reflections that correspond to the DPP-4T-BOC_2 confirms the successful completion of decarboxylation reactions and the formation of DPP-4T.[27]

Figure 5 represents the increase of the amorphous halo upon decreasing the isothermal decarboxylation temperature. The percentage of crystallinity of DPP-4T powder obtained through

dx.doi.org/10.1021/cg401625p | *Cryst. Growth Des.* 2014, 14, 339−349

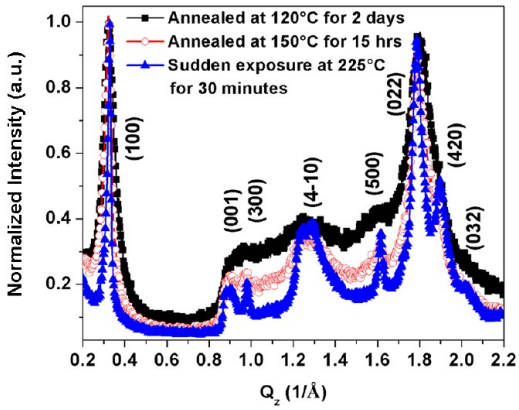

Figure 5. Powder pattern of DPP-4T obtained by isothermally decarboxylating the precursor at various temperatures.

the thermal conversion of its precursor with various thermal treatments was extracted from the respective powder patterns using the relation given in the Supporting Information (SE1).[28] The crystallinity of DPP-4T powder increases from 28% to 48% while increasing the isothermal decarboxylation temperature from 120 to 225 °C (Table 2). In addition, the full width at half-maximum (fwhm) of the Bragg reflections was also noticed to increase on reducing the decarboxylation temperature (Table 2). The increase in fwhm of Bragg reflections could be attributed to the decrease in crystallite size as reducing the decarboxylation temperature as observed through the AFM images of DPP-4T films (see later). The decrease in crystallinity of DPP-4T together with the decarboxylation temperature may be caused by the decreased decarboxylation rate (Table 1). For example, the precursor decarboxylated by heating up to 225 °C with various heating rates also reveals the decrease in crystallinity with the heating rate; i.e., the crystallinity of DPP-4T is decreasing from 49% to 34% while decreasing the heating rate from 50 to 0.1 °C/min (Table 3). The decrease in crystallinity of DPP-4T together with the heating rate as well as the isothermal decarboxylation temperature could be attributed to the augmentation in trapping of gaseous byproducts, such as isobutylene and CO_2, as observed through FTIR (see later).[19]

Table 2. Percentage of Crystallinity and fwhm of (100) Bragg Reflections of the DPP-4T Powders Obtained by Decarboxylating the Precursor Isothermally at Various Temperatures

decarboxylation temperature (°C)	time duration (h)	fwhm (deg) ± 0.01	percentage of crystallinity (±3)
120	48	0.93	28
150	15	0.57	35
225 (sudden exposure)	0.5	0.27	46

Table 3. Percentage of Crystallinity of DPP-4T Powders Obtained by Decarboxylating the Precursor Powders by Heating up to 225 °C with Various Heating Rates

heating rate (°C/min)	percentage of crystallinity (±3)
0.1	34
1	37
10	39
30	44
50	49

The powder pattern of thermally synthesized DPP-4T was not good enough to solve the crystal structure or to index the powder patterns. Therefore, efforts have been taken to grow single crystals of DPP-4T via different techniques, such as sublimation, slow cooling, slow evaporation, and liquid/liquid diffusion, but those were not successful. Moreover, the poor solubility of DPP-4T in most of the organic solvents suppresses the growth of single crystals by employing various solution growth techniques. Therefore, the powder pattern of DPP-4T was used to index the scattering patterns. To do so, DPP-4T powder with a unique polymorphic phase has been synthesized (Figure S6, Supporting Information). The powder pattern of DPP-4T recrystallized using DMSO matches well with the thermally synthesized DPP-4T from its precursor. Therefore, the powder pattern of DPP-4T recrystallized using DMSO was used to index the Bragg reflections (Figure S6c, Supporting Information). It was not possible to refine the crystal structure because of the presence of two culminated peaks at Q_z = 0.88 and 1.26 $Å^{-1}$ as well as the poor crystallinity. However, the preliminary investigation shows that the crystal structure belongs to the triclinic centrosymmetric space group $P\bar{1}$ with $Z = 4$ (a = 19.78 Å, b = 11.95 Å, and c = 7.43 Å; α = 73.56°, ß = 96.4°, and γ = 106.33°). The other polymorphic phase was also separated by subliming the DPP-4T at 275 °C under 10^{-6} Torr. It sublimes only under high vacuum (Figure S6b, Supporting Information). The second phase belongs to the monoclinic unit cell with the lattice parameters a = 15.70 Å, b = 20.05 Å, and c = 5.65 Å; ß = 93.17°. Further work is going on to solve the crystal structure by improving the crystalline quality of DPP-4T powder. However, the main goal of this article is to address the role of the solubilizing group removal rate on the crystallinity as well as the morphology of the films rather than solving the crystal structure of DPP-4T.

FTIR Investigations of Thin Films. FTIR spectra of DPP-4T films, obtained through the thermal conversion of its precursor films, were recorded to understand the cause of decrease in crystallinity with the heating rate as well as the isothermal decarboxylation temperature. The corresponding IR absorption spectra are shown in Figure 6. The spectra were normalized to the C═C stretching vibration (1611 cm^{-1})[33,34] and then shifted along the ordinate axis by adding some values for clearer presentation. In the case of DPP-4T-BOC_2 (precursor) film, an absorption band was observed at 2982 cm^{-1} that corresponds to the asymmetric CH_3 stretching vibration present in the *t*-BOC. After the decarboxylation, new bands were observed at 2917 and 2850 cm^{-1} that correspond to the asymmetric and symmetric CH_2 stretching vibrations, respectively (Figure 6a).[35] The increase in intensity of those peaks confirms the increase in trapping of isobutylene inside the lattice with decreasing the heating rate. The band observed at 1539 cm^{-1} corresponds to the H-bonded N−H bending vibration between the N−H and C═O groups.[34] The absorption intensity of this N−H bending vibration increases while decreasing the heating rate from 50 to 0.1 °C/min (Figure 6a). For further clarification, the FTIR spectra of the films decarboxylated isothermally at 120, 150, and 225 °C were recorded and are shown in Figure 6b. The same tendency can be observed, i.e., the increase in absorption of N−H bending vibration as well as the symmetric and asymmetric stretching vibrations of CH_2 while decreasing the isothermal decarbox-

dx.doi.org/10.1021/cg401625p | Cryst. Growth Des. 2014, 14, 339−349

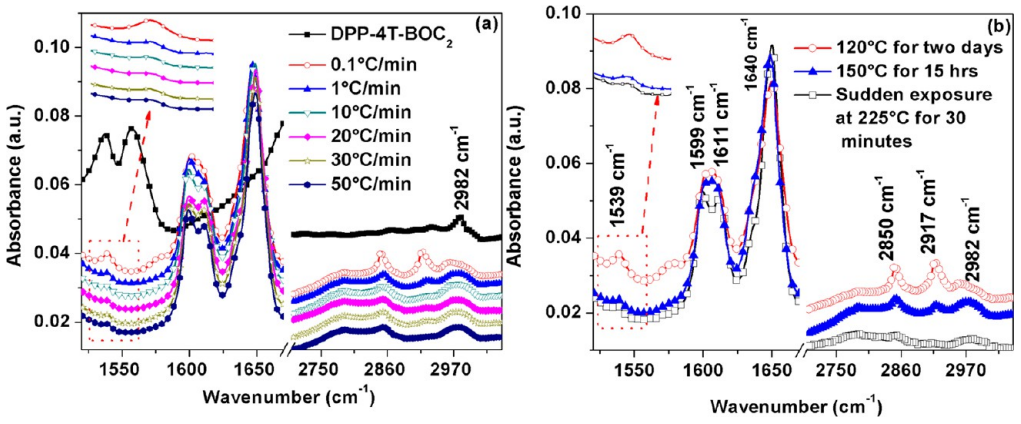

Figure 6. FTIR spectra of DPP-4T films obtained from DPP-4T-BOC_2 through the thermochemical process: (a) with different heating rates (heated until 225 °C) and (b) by decarboxylating isothermally at various temperatures.

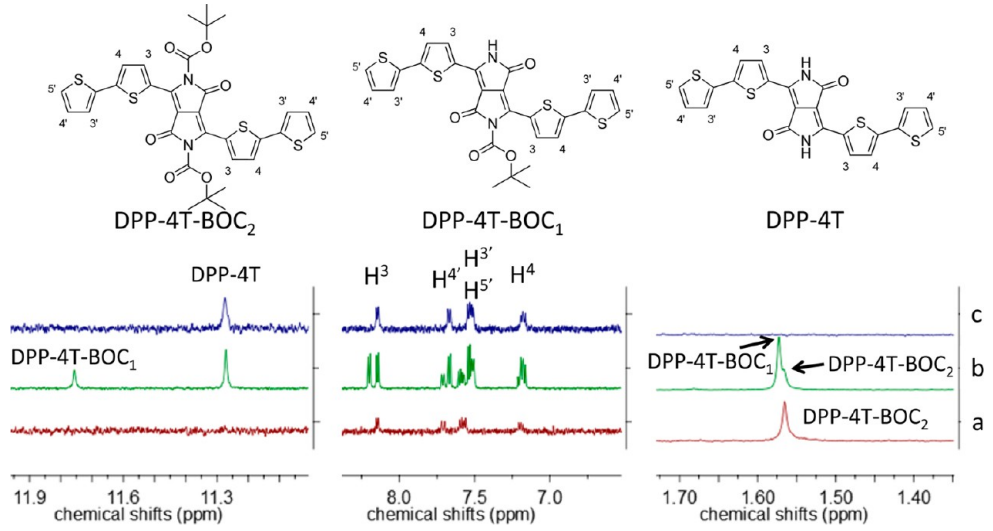

Figure 7. ^{1}H NMR spectra of (a) DPP-4T-BOC_2 and (b, c) DPP-4T-BOC_2 isothermally decarboxylated at 120 °C for 3 and 48 h, respectively. This is only the magnification of NH, aromatic, and *t*-BOC proton's chemical shift regions. The whole spectra can be found in the Supporting Information (Figure S8).

ylation temperature. It clearly envisages the augmentation in trapping of gaseous byproducts inside the DPP-4T crystallites with decreasing the *t*-BOC removal rate. However, it was not possible to confirm the trapping of CO_2 inside the lattice because of the contribution of atmospheric CO_2.

Wang et al. have documented that the absorption intensity of H-bonded N−H bending vibration increases upon heating the polyurethanes because of increased N−H···O═C H-bond length.[34] Therefore, the increase in intensity of the N−H bending vibration on decreasing either the heating rate or the isothermal decarboxylation temperature may be due to the increment in C═O···H−N hydrogen bond length, caused by the trapped gaseous byproducts. The poor C═O···H−N hydrogen bonding eventually results in a blue shift in the UV−vis absorption spectra (Figure S7, Supporting Information), as observed by Adachi et al. in the case of DPP-phenyl.[8,36] It is evident that the trapped gaseous byproducts can eventually hinder the close-packing of DPP-4T and thereby increases the amorphicity of the films and powders, as observed through the X-ray diffraction analyses (Figures 4 and 5). Recently, Sun et al. reported that the gaseous byproducts can be easily volatilized from the films rather than the powder, during the decomposition of the solubilizing group.[19] Our investigation clearly depicts that the volatilization of gaseous byproducts during the decomposition of solubilizing groups mainly depends on the decarboxylation rate. The evolution of N−H vibration, after the decarboxylation process, confirms the formation of N−H bonds during the decarboxylation of *t*-BOC.

Solution ^{1}H NMR Analysis of DPP-4T-BOC_2 Powder Decarboxylated Isothermally at 120 °C for Various Time Scales. The NMR spectra of DPP-4T-BOC_2 powder isothermally decarboxylated at 120 °C for various time scales were recorded to have a clear idea about the thermal elimination mechanism of the solubilizing groups. To do so, ^{1}H NMR spectra of the as-synthesized and the DPP-4T-BOC_2 isothermally decarboxylated at 120 °C for 3 and 48 h were recorded by dissolving it in DMSO-d_6 (Figure 7). The DPP-4T-BOC_2 has few signals: (i) the peak observed at δ = 1.57 ppm belongs to the methyl groups present in the *t*-BOC moieties, and (ii) the four other peaks observed in the aromatic part at δ = 7.20, 7.57, 7.71, and 8.14 ppm correspond to the protons H^4, combined H^3 and $H^{5'}$, $H^{4'}$, and H^3, respectively (Figure 7a). The precursor powder decarboxylated at 120 °C for 3 h indicates that the decarboxylation of *t*-BOC was not complete and it contains the mixture of three compounds, i.e., DPP-4T-BOC_2, *tert*-butyl-3,6-di(2,2′-bithiophen-5-yl)-1,4-

dx.doi.org/10.1021/cg401625p | *Cryst. Growth Des.* 2014, 14, 339−349

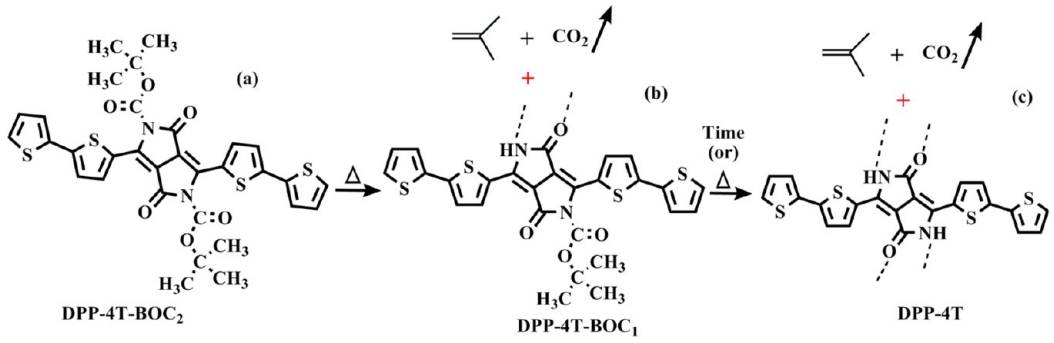

Figure 8. Illustration of the asynchronous decarboxylation of both the *t*-BOCs from DPP-4T-BOC_2 upon thermal conversion.

dioxo-4,5-dihydropyrrolo[3,4-*c*]pyrrole-2(1*H*)-carboxylate (DPP-4T-BOC_1), and DPP-4T. Indeed, the observations of (i) two peaks at δ = 1.57 ppm indicate the coexistence of both the DPP-4T-BOC_2 and DPP-4T-BOC_1, and (ii) two peaks observed at δ = 11.27 and 11.76 ppm correspond to the NH protons of DPP-4T and DPP-4T-BOC_1 derivatives, respectively (Figure 7b). The absence of any signal at δ =1.57 ppm in DPP-4T-BOC_2 powder annealed at 120 °C for 2 days, which corresponds to the methyl group of *t*-BOC, confirms the complete elimination of the solubilizing groups (Figure 7c). In addition, a single peak observed in the region of NH protons confirms the completion of the decarboxylation reaction. The four peaks observed in the aromatic region at δ = 7.17, 7.53, 7.37, and 8.14 ppm correspond to the protons of H^4, combined H^3 and $H^{5'}$, $H^{4'}$, and H^3, respectively. These observations are consistent with the formation of the N−H bond upon thermal elimination of *t*-BOC as observed through FTIR.

The NMR analysis clearly depicts that both the *t*-BOCs do not cleave simultaneously. Nevertheless, it decarboxylates completely while increasing the duration of the isothermal decarboxylation process or the temperature. It is schematically illustrated in Figure 8. Such an asynchronous decarboxylation of both the *t*-BOCs can decrease the crystallinity of DPP-4T because of the trapping of *t*-BOC inside the DPP-4T network, which can decarboxylate later and get stuck into the lattice. The trapping of *t*-BOC inside the DPP-4T network can increase while decreasing the heating rate as well as the isothermal decarboxylation temperature because of the amplified time difference between the decarboxylation of both the *t*-BOCs. It can subsequently hinder the bonding between the neighboring molecules as well as the growth of DPP-4T crystallites as observed through FTIR and AFM analyses, respectively.

Morphological Investigations of DPP-4T. *AFM Analysis of Thin Films.* AFM height images of DPP-4T films, obtained from their precursor films through thermochemical process, were collected to understand the role of *t*-BOC removal rate on their morphology by varying the heating rate as well as the isothermal decarboxylation temperature. More than four AFM height images were recorded at various places of the DPP-4T films in order to get a proper statistical length of the crsyatllites. The length of an individual DPP-4T crystallite was measured using the software "Nanaoscope SPM", and the corresponding histogram is shown on the right side of the appropriate figures (Figure 9). The average length of the crystallites is given in Table 4. The lengths of DPP-4T crystallites were noted to increase more or less linearly with the heating rates applied (Figure 9b); i.e., the average length of the crystallites is increased from 345 to 976 nm while increasing the heating rate from 0.1 to 50 °C/min. Moreover, the roughnesses of the films were also found to increase from 32 to 75 nm while increasing the heating rate from 0.1 to 50 °C/min (Table 4). It might be due to the evolution cracks and holes during the decomposition of the solubilizing groups, as observed through the optical microscope (Figure S9, Supporting Information).[7]

This increment in DPP-4T crystallite size together with the heating rate of the decarboxylation process brought us two major questions: (i) Does the crystallite size depend on the duration of annealing? (ii) Does it depend on the crystallization of DPP-4T-BOC_2 during heating?[24] The first question can be easily answered, because, obviously, the film decarboxylated with the heating rate of 0.1 °C/min will take more time than the one heated with the rate of 50 °C/min to reach the set point value (225 °C). However, here, the film decarboxylated with the heating rate of 0.1 °C/min (345 nm) produces smaller crystallites than the one heated with the rate of 50 °C/min (975 nm). Therefore, it is evident that the increase of crystallite size together with the heating rate does not depend on the duration of annealing.

To answer the second question, two different methodologies were employed. At first, a precursor film was decarboxylated by directly exposing at 225 °C for 30 min in order to avoid the crystallization of DPP-4T-BOC_2 during heating. Interestingly, it ends up with the average crystallite length of 828 nm (Figure 10). In addition, two other precursor films were also decarboxylated isothermally at 120 and 150 °C by waiting for 2 days and 15 h, respectively. Eventually, the average length of the crystallites reduced from 457 to 186 nm while decreasing the isothermal decarboxylation temperature from 150 to 120 °C (Table 5).

In Situ Microscopic Investigations of DPP-4T-BOC_2 Single Crystals during Heating. As a second step, single crystals of DPP-4T-BOC_2 were decarboxylated under the optical microscope. For this purpose, single crystals of DPP-4T-BOC_2 were grown by the liquid/liquid diffusion technique as reported by us earlier.[27] The POM and the optical microscopic images of DPP-4T-BOC_2 single crystals are shown in the first and second columns of Figure S10 (Supporting Information), respectively. The single crystals of DPP-4T-BOC_2 were heated up to 225 °C with the heating rates of 0.1 and 30 °C/min, and the snapshots have been taken at every 10 min and 10 s, respectively. Because of the limitation of hot plate, it was not possible to exceed the heating rate of 30 °C/min. Both the crystals were noted to bend during the decarboxylation process, but the crystal decarboxylated with the heating rate of 0.1 °C/min bends much more than the one decarboxylated with the heating rate of 30 °C/min (Figure S10e,f and the movies are presented in the Supporting Information, SMV1 and SMV2). On the contrary, the crystal decarboxylated with the heating rate of 30 °C/min

dx.doi.org/10.1021/cg401625p | *Cryst. Growth Des.* 2014, 14, 339−349

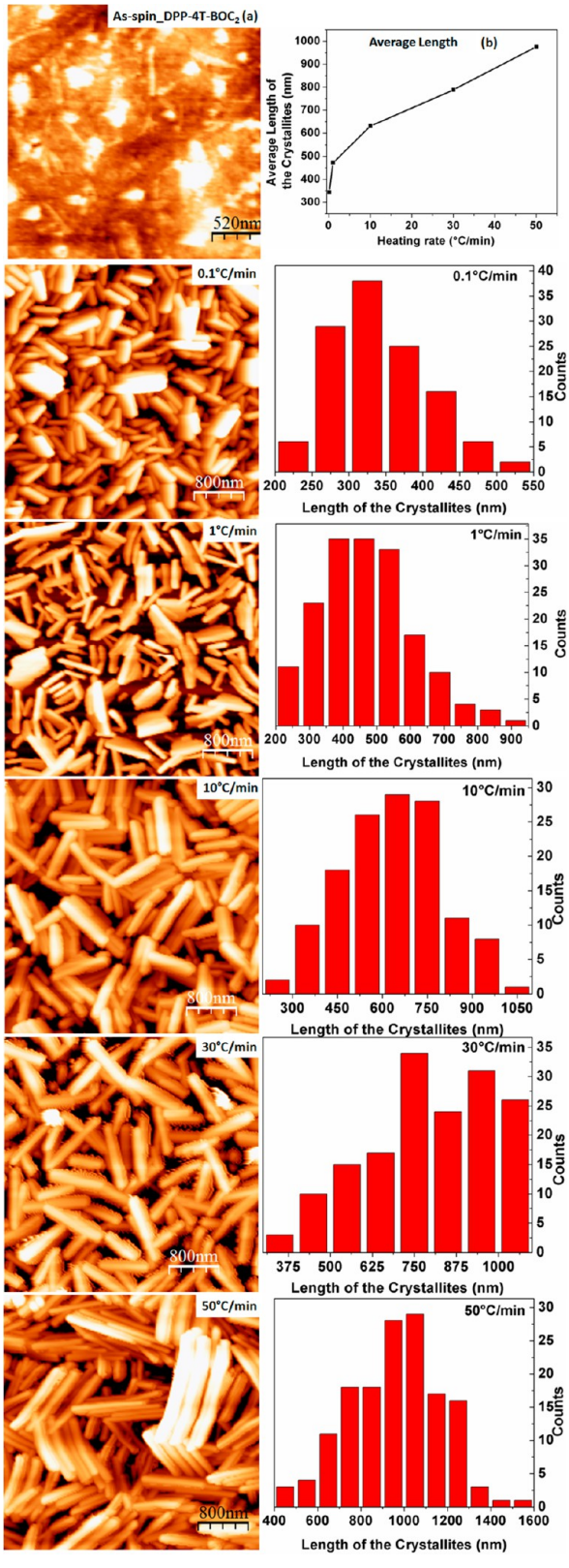

Figure 9. AFM height images of DPP-4T thin films obtained through the thermal conversion of their precursor with various heating rates (heated up to 225 °C) (left column), and the right-side column shows the histograms of the length of the crystallites. (a) AFM height image of as-spin-coated DPP-4T-BOC_2. Panel (b) depicts the increase in length of the DPP-4T crystallites with the heating rate.

Table 4. Average Crystallite Length and Surface Roughness of DPP-4T Films Obtained through the Thermal Conversion of Their Precursor Films with Various Heating Rates As Observed by AFM (Heated up to 225 °C)

heating rate (°C/min)	average crystallite length (nm) (±2 nm)	surface roughness (nm) (±5 nm)
0.1	345	32
1	472	47
10	631	50
30	789	57
50	976	75

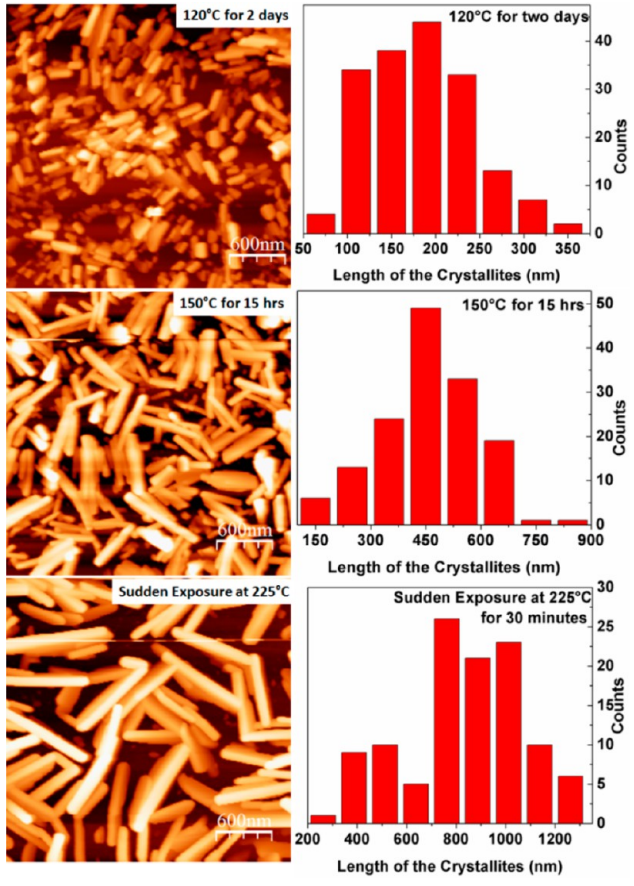

Figure 10. AFM height images of DPP-4T films obtained by decarboxylating the precursor films isothermally at various temperatures (left column), and the right-side column shows the histograms of the length of the crystallites.

Table 5. The Influence of Isothermal Decarboxylation Temperature on the Crystallite Length and Surface Roughness of DPP-4T Films

decarboxylation temperature (°C)	time duration (h)	average crystallite length (nm) (±2 nm)	surface roughness (nm) (±5 nm)
120	48	186	43
150	15	457	63
225 (sudden exposure)	0.5	828	78

crumbles into smaller crystallites (Figure S10e, Supporting Information). The same behavior was also observed in the single crystals decarboxylated under a thermal gradient with various pulling rates; i.e., the crystal pulled with the rate of 25

dx.doi.org/10.1021/cg401625p | Cryst. Growth Des. 2014, 14, 339−349

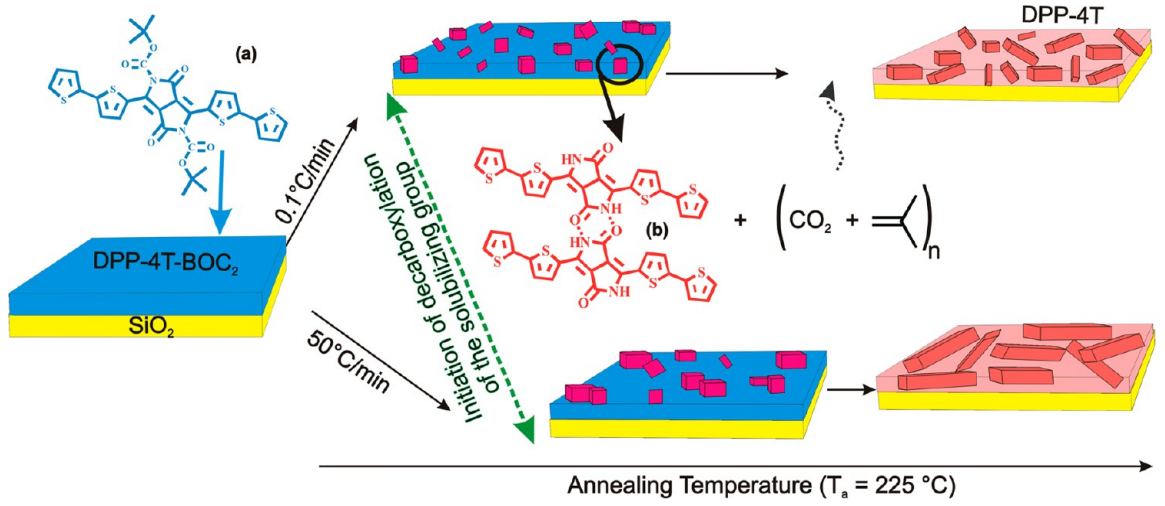

Figure 11. Illustration of the role of heating rate on the initiation of decarboxylation of the solubilizing group and its impact on their ultimate grain size.

μm/s cracks into small crystallites than the one pulled with the rate of 1 μm/s (not shown). The augumentation in bending of the crystals while decreasing the heating rate of the decarboxylation process maybe due to the stress induced by the trapped gaseous byproducts during the decomposition of *t*-BOC, as observed through FTIR (Figure 6). However, it clarifies that the ultimate crystallite size of DPP-4T does not depend on the preexisting crystallites in the DPP-4T-BOC_2 film (Figure 9a). If it is the case, then the film decarboxylated with the heating rate of 50 °C/min must provide smaller crystallites than the one heated with the rate of 0.1 °C/min. It is worth mentioning that the crystallinity of DPP-4T-BOC_2 does not improve much upon heating as compared to the SVA-films.[27]

The overall findings clearly depict that the ultimate crystallite size depends neither on the crystallization of DPP-4T-BOC_2 during heating nor on the duration of annealing, but it mostly depends on the removal rate of the solubilizing group. The decrease in DPP-4T crystallite size together with the heating rate of the decarboxylation process as well as the isothermal decarboxylation temperature may be caused by the initiation of multiple nucleations. It is schematically illustrated in Figure 11. The initiation of multiple nucleations may be caused by the following two reasons: (i) lack of molecular migrations and (ii) the absence of neighboring DPP-4T molecules to make bonds, i.e., the solubilizing group free DPP-4T-BOC_2. Soeda et al. have succeeded to grow single crystalline platelets of DNTT and pentacene from their precursor solution during the removal of the solubilizing group via heat treatment.[13] On the contrary, the same pentacene films obtained from their precursor through thermochemical process end up with smaller crystallites.[23] It might be due to the reduced migration of molecules in the solid state as compared to the liquid state. However, the neighboring molecules must be free to make bonds, which facilitate the growth of the crystallites.

According to TGA, around 7.1 mg of precursor takes 159 and 22 s to complete the decarboxylation reaction while heating with the rates of 5 and 50 °C/min, respectively (Table 1). Moreover, ≈6 mg of DPP-4T-BOC_2 powder isothermally decarboxylated at 120 and 150 °C takes 2357 and 158 min to finish the decarboxylation reaction, respectively. So, the decrease in decarboxylation rate of DPP-4T-BOC_2 on decreasing either the heating rate or the isothermal decarboxylation temperature can suppress the growth of DPP-4T crystallites along one direction because of the absence of simultaneous decarboxylation of both the *t*-BOCs, as observed through NMR (Figures 7 and 8). It can eventually increase the nucleation density of DPP-4T because of the lack of molecular migration in the solid state as well as the absence of neighboring DPP-4T to make bonds (Figure 11). It has been documented that the DPP-phenyl slides during the decarboxylation in order to make stronger $\pi-\pi$ interations and N−H···O═C hydrogen bonds with the neighboring molecules.[8] Therefore, the asynchronous decarboxylation of both the *t*-BOCs can eventually suppress the sliding of DPP-4T and the formation of bonds between the neighboring molecules, which can eventually suppress the growth as well the coherence in lattice spacing. On the contrary, the increase in decarboxylation rate together with the heating rate can increase the crystallite size because of the possibility of simultaneous decarboxylation of both the *t*-BOCs as well as the presence of neighboring (DPP-4T) molecules to make hydrogen bonds and $\pi-\pi$ interactions, which mainly governs the planarity of DPP crystallites.[36]

■ CONCLUSIONS

In summary, the morphology of thermally synthesized solubilizing group free organic small molecules can be altered by varying the solubilizing group removal rate. The solubilizing group removal rate can be increased by increasing either the heating rate or the isothermal decarboxylation temperature of the decarboxylation process. For example, the solubilizing group free thermally synthesized dithiophene-DPP-dithiophene (DPP-4T) from its precursor film by heating to 225 °C depicts the increase of crystallite size from 344 to 976 nm while increasing the heating rate from 0.1 to 50 °C/min. Moreover, the crystallinity of DPP-4T also increases with the heating rate. The DPP-4T tends to make N−H···O═C hydrogen bonds and $\pi-\pi$ interactions during the removal of the solubilizing group (*t*-butoxycarbonyl (*t*-BOC)). Therefore, eventually, the decrease in solubilizing group removal rate with the heating rate of the decarboxylation process can decrease the ultimate crystallite size because of the absence of neighboring DPP-4T molecules to make N−H···O═C hydrogen bonds and $\pi-\pi$ interactions. Moreover, the decrease in solubilizing group

dx.doi.org/10.1021/cg401625p | *Cryst. Growth Des.* 2014, 14, 339−349

removal rate together with the heating rate can increase the time interval between the decarboxylation of both the *t*-BOCs, which are grafted on a single DPP core. This can also decrease the crystallite size and crystallinity of the final films because of the hindrance in growth along one direction as well as the trapping of *t*-BOC inside the DPP-4T network. On the contrary, as we increase the heating rate or the isothermal decarboxylation temperature, the volatilized compounds can easily escape from the lattice because of the profound decarboxylation rate and the probability of simultaneous decarboxylation of both the *t*-BOCs, which can facilitate the growth of the crystallites by making bonds with the neighboring molecules. This is the first time we have shown that the solubilizing group removal rate plays an important role on the ultimate crystallite size and crystallinity of the final films, which are the crucial factors that govern the electrical and optical properties of the materials. Such an increment in trapping of gaseous byproducts while decreasing the solubilizing group removal rate makes a blue shift in the UV−vis absorption spectra because of the increased N−H···O═C hydrogen bond length.

■ ASSOCIATED CONTENT

Supporting Information

X-ray diffraction patterns of DPP-4T-BOC_2; POM images of as-spin-coated and SVA DPP-4T-BOC_2 films; in situ diffraction patterns of DPP-4T-BOC_2 upon heating; X-ray diffraction patterns of DPP-4T films; X-ray powder patterns of sublimed and recrystallized DPP-4T powders; UV−vis absorption spectra of DPP-4T films obtained through the thermal conversion of their precursor films; ^{1}H NMR spectra; light microscopic images of DPP-4T films; POM and light microscopic images of DPP-4T-BOC_2 single crystals; videos of decarboxylation of DPP-4T-BOC_2 single crystals; and percentage of crystallinity and electron density calculations. This material is available free of charge via the Internet at http://pubs.acs.org.

■ AUTHOR INFORMATION

Corresponding Author

*E-mail: sthankar@ulb.ac.be, tsshabi@gmail.com.

Notes

The authors declare no competing financial interest.

■ ACKNOWLEDGMENTS

The authors are thankful to the ARC program of the Communauté Française de Belgique (Grant No. 20061) for the financial support.

■ REFERENCES

(1) Chandran, D.; Lee, K.-S. *Macromol. Res.* **2013**, *21*, 272−283.
(2) Chen, L.; Deng, D.; Nan, Y.; Shi, M.; Chan, P. K.; Chen, H. *J. Phys. Chem. C* **2011**, *115*, 11282−11292.
(3) Lee, J.; Han, A.; Hong, J.; Seo, J. H.; Oh, J. H.; Yang, C. *Adv. Funct. Mater.* **2012**, *22*, 4128−4138.
(4) Qu, S.; Tian, H. *Chem. Commun.* **2012**, *48*, 3039−3051.
(5) Kim, C.; Liu, J.; Lin, J.; Tamayo, A. B.; Walker, B.; Wu, G.; Nguyen, T.-Q. *Chem. Mater.* **2012**, *24*, 1699−1709.
(6) Zhou, E.; Yamakawa, S.; Tajima, K.; Yang, C.; Hashimoto, K. *Chem. Mater.* **2009**, *21*, 4055−4061.
(7) Zambounis, J. S.; Hao, Z.; Iqbal, A. *Nature* **1997**, *388*, 131−132.
(8) Wallquist, O.; Lenz, R. *Macromol. Symp.* **2002**, *187*, 617−630.
(9) Gomez, E. D.; Barteau, K. P.; Wang, H.; Toney, M. F.; Loo, Y.-L. *Chem. Commun.* **2011**, *47*, 436−438.
(10) Dikundwar, A. G.; Dutta, G. K.; Guru Row, T. N.; Patil, S. *Cryst. Growth Des.* **2011**, *11*, 1615−1622.
(11) Lee, H. S.; Cho, J. H.; Cho, K.; Park, Y. D. *J. Phys. Chem. C* **2013**, *117*, 11764−11769.
(12) Sergeyev, S.; Pisula, W.; Geerts, Y. H. *Chem. Soc. Rev.* **2007**, *36*, 1902−1929.
(13) Soeda, J.; Okamoto, T.; Hamaguchi, A.; Ikeda, Y.; Sato, H.; Yamano, A.; Takeya, J. *Org. Electron.* **2013**, *14*, 1211−1217.
(14) Søndergaard, R.; Helgesen, M.; Jørgensen, M.; Krebs, F. C. *Adv. Energy Mater.* **2011**, *1*, 68−71.
(15) Han, X.; Chen, X.; Holdcroft, S. *Chem. Mater.* **2009**, *21*, 4631−4637.
(16) Yamada, H.; Okujima, T.; Ono, N. *Chem. Commun.* **2008**, 2957−2974.
(17) Watanabe, M.; Chen, K.-Y.; Chang, Y. J.; Chow, T. J. *Acc. Chem. Res.* **2013**, *46*, 1606−1615.
(18) Matsuo, Y.; Sato, Y.; Niinomi, T.; Soga, I.; Tanaka, H.; Nakamura, E. *J. Am. Chem. Soc.* **2009**, *131*, 16048−16050.
(19) Sun, B.; Hong, W.; Aziz, H.; Li, Y. *J. Mater. Chem.* **2012**, *22*, 18950−18955.
(20) Gagnon, D.; Capistran, J.; Karasz, F.; Lenz, R.; Antoun, S. *Polymer* **1987**, *28*, 567−573.
(21) Watanabe, M.; Chang, Y. J.; Liu, S.-W.; Chao, T.-H.; Goto, K.; Islam, M. M.; Yuan, C.-H.; Tao, Y.-T.; Shinmyozu, T.; Chow, T. J. *Nat. Chem.* **2012**, *4*, 574−578.
(22) Afzali, A.; Dimitrakopoulos, C. D.; Breen, T. L. *J. Am. Chem. Soc.* **2002**, *124*, 8812−8813.
(23) Shaw, J. E.; Stavrinou, P. N.; Anthopoulos, T. D. *Adv. Mater.* **2013**, *25*, 552−558.
(24) Salammal, S. T.; Mikayelyan, E.; Grigorian, S.; Pietsch, U.; Koenen, N.; Scherf, U.; Kayunkid, N.; Brinkmann, M. *Macromolecules* **2012**, *45*, 5575−5585.
(25) Snaith, H. J.; Arias, A. C.; Morteani, A. C.; Silva, C.; Friend, R. H. *Nano Lett.* **2002**, *2*, 1353−1357.
(26) MacLean, E. J.; Tremayne, M.; Kariuki, B. M.; Cameron, J. R.; Roberts, M. A.; Harris, K. D. *Cryst. Growth Des.* **2009**, *9*, 853−857.
(27) Salammal, S. T.; Balandier, J.-Y.; Arlin, J.-B.; Olivier, Y.; Lemaur, V.; Cornil, J.; Kennedy, A. R.; Geerts, Y. H.; Chattopadhyay, B. *J. Phys. Chem. C* **2013**, Submitted.
(28) Mo, Z.; Zhang, H. *J. Macromol. Sci., Part C: Polym. Rev.* **1995**, *35*, 555−580.
(29) Vonk, C. *J. Appl. Crystallogr.* **1973**, *6*, 148−152.
(30) Als-Nielsen, J.; McMorrow, D. *Elements of Modern X-Ray Physics*; John Wiley & Sons Inc: Chichester, U.K., 2001.
(31) Schweicher, G.; Paquay, N.; Amato, C.; Resel, R.; Koini, M.; Talvy, S.; Lemaur, V.; Cornil, J. r. m.; Geerts, Y.; Gbabode, G. *Cryst. Growth Des.* **2011**, *11*, 3663−3672.
(32) Bundgaard, E.; Hagemann, O.; Bjerring, M.; Nielsen, N. C.; Andreasen, J. W.; Andreasen, B.; Krebs, F. C. *Macromolecules* **2012**, *45*, 3644−3646.
(33) Behnke, M.; Tieke, B. *Langmuir* **2002**, *18*, 3815−3821.
(34) Wang, F. C.; Feve, M.; Lam, T. M.; Pascault, J. P. *J. Polym. Sci., Part B: Polym. Phys.* **1994**, *32*, 1305−1313.
(35) Lu, R.; Gan, W.; Wu, B.-h.; Zhang, Z.; Guo, Y.; Wang, H.-f. *J. Phys. Chem. B* **2005**, *109*, 14118−14129.
(36) Adachi, M.; Nakamura, S. *J. Phys. Chem.* **1994**, *98*, 1796−1801.